size of this region is roughly the length between the contacts.

Each peak therefore corresponds to resonant tunneling though a coherent molecular state that extends for up to hundreds of nanometers in a localized region within the nanotube bundle. Furthermore, the amplitudes of some isolated peaks approach the theoretical maximum for single-electron transport of e^2/h. This amplitude is only possible if the barriers that confine this state at either end are approximately equal and there is no other significant resistance in series with the localized region. These requirements are consistent with the barriers being at the contacts between the metal leads and the rope. It is also possible that the barriers are within the rope, in which case the metal-rope contacts must be almost ideal so as not to reduce the maximum conductance from e^2/h (*17*). Variation in the coupling to each lead from level to level can account for the varying peak sizes apparent in Fig. 2.

Although the above interpretation accounts for the major features in the data, many interesting aspects of this system remain to be explored. First, one would like to establish absolutely that transport is indeed occurring predominantly along a single tube. Second, it should be determined whether all details of the data can be explained within the simple CB model discussed above, because Coulomb interactions may significantly modify the low-energy states from simple 1D noninteracting levels (*18*). Of great interest would be measurements of disorder-free tubes, where the intrinsic conducting properties of the tube can be measured without the complications of single-electron charging. To address these issues, experiments on individual single-walled tubes are highly desirable, and progress is being made in this direction (*19*). Yet another important experiment would be to measure directly the intertube coupling by making separate electrical contact to two adjacent tubes.

REFERENCES AND NOTES

1. For a review, see H. Grabert and M. H. Devoret, Eds., *Single Charge Tunneling* (Plenum, New York, 1991); M. A. Kastner, *Phys. Today* **46**, 24 (January 1993); L. P. Kouwenhoven and P. L. McEuen, in *Nanoscience and Technology*, G. Timp, Ed. (AIP Press, New York, in press).
2. S. Iijima, *Nature* **354**, 56 (1991); for a recent review, see T. W. Ebbesen, *Phys. Today* **49**, 26 (June 1996).
3. R. Saito, M. Fujita, G. Dresselhaus, M. S. Dresselhaus, *Appl. Phys. Lett.* **60**, 2204 (1992); N. Hamada, S. Sawada, A. Oshiyama, *Phys. Rev. Lett.* **68**, 1579 (1992).
4. A. Thess *et al.*, *Science* **273**, 483 (1996).
5. L. Langer *et al.*, *Phys. Rev. Lett.* **76**, 479 (1996).
6. H. Dai, E. W. Wong, C. M. Lieber, *Science* **272**, 523 (1996).
7. T. W. Ebbesen *et al.*, *Nature* **382**, 54 (1996); A. Yu. Kasumov, I. I. Khodos, P. M. Ajayan, C. Colliex, *Europhys. Lett.* **34**, 429 (1996).
8. J. E. Fischer *et al.*, *Phys. Rev. B* **55**, 4921 (1997).
9. D. Bernaerts *et al.*, preprint (1996); J. M. Cowley, P. Nikolaev, A. Thess, R. E. Smalley, *Chem. Phys. Lett.* **265**, 379 (1997).
10. The level spacing can be determined from the data in Fig. 3 by two means. The first means is to measure the separation between features in V_g and use the conversion factor $\alpha = V_{max}/\Delta V_g$. The second is to measure the separation between the features in V and use the slopes of the lines defining the Coulomb gap to infer $\alpha_L = C_L/C$ and $\alpha_R = C_R/C$. For more information, see (*1*).
11. H.-Y. Zhu, D. J. Klein, T. G. Schmalz, N. H. Rubio, N. H. March, preprint (1996).
12. L. X. Benedict, S. G. Louie, M. L. Cohen, *Phys. Rev. B* **52**, 8541 (1995).
13. Other measurements on these samples also support the notion that transport is through individual decoupled tubes. In four-terminal measurements of the ropes at temperatures $>$ 30 K (where the rope resistance becomes much less than the voltage-probe impedance and reliable four-terminal measurements are possible), nonlocal voltages have been observed. For example, referring to the AFM image shown in Fig. 1, a voltage can appear between the terminals 1 and 2 in response to a current flowing between contacts 3 and 4. Such nonlocal effects are possible if different contacts make contact to different tubes and the intertube coupling is small. Current injected into 4 in a particular tube that is not well connected to 3 can arrive at contact 1 or 2, producing a nonlocal response.
14. Individual tubes within a rope have chiral angles within 10° of the achiral (10, 10) tube with roughly 30 to 40% of the sample being (10, 10) tubes (*9*). The indices of tubes consistent with the experimental constraints on chirality and radius (*4*) are (10, 10), (9, 11), (8, 12), (7, 13), and the opposite-handed twins. The gap of the (7, 13) tube is small and likely does not survive intertube interactions, but the gaps of the (9, 11) and (8, 12) tubes are about 0.5 eV, which is probably large enough to maintain semiconducting behavior within the rope.
15. L. Chico, L. X. Benedict, S. G. Louie, M. L. Cohen, *Phys. Rev. B* **54**, 2600 (1996); L. Chico *et al.*, *Phys. Rev. Lett.* **76**, 971 (1996).
16. C. L. Kane and E. J. Mele, *Phys. Rev. Lett.*, in press.
17. The large peak heights, combined with the fact that the room-temperature conductance of the center segment is also approximately e^2/h, imply that good electrical contact has been made between the metal leads and part of the rope.
18. Y. A. Krotov, D.-H. Lee, S. G. Louie, preprint (cond-mat/9611073, available on the Internet from the e-Print archive at xxx.lanl.gov); L. Balents and M. P. A. Fisher, preprint (cond-mat/9611126, available from the e-Print archive at xxx.lanl.gov).
19. S. Tans, preprint (1997).
20. We would like to acknowledge useful discussions with V. Crespi, M. Cohen, D. H. Lee, and S. Louie. We are also indebted to S. Tans for communicating his unpublished results of measurements on nanotubes and emphasizing the importance of a gate voltage. Supported by the U.S. Department of Energy, under contract DE-AC03-76SF00098, and by the Office of Naval Research, order N00014-95-F-0099.

13 December 1996; accepted 25 February 1997

Origin of the High-Frequency Doublet in the Vibrational Spectrum of Vitreous SiO_2

Johannes Sarnthein, Alfredo Pasquarello,* Roberto Car

The vibrational properties of amorphous SiO_2 were studied within first-principles density functional theory. The calculated spectrum is in good agreement with neutron data, showing, in particular, a double peak in the high-frequency region. This doublet results from different local modes of the tetrahedral subunits and cannot be ascribed to a longitudinal-optic–transverse-optic (LO-TO) effect. This solves a long-standing controversy about the origin of the doublet in neutron spectra. A LO-TO splitting is recovered only when the long-wavelength limit is probed, as in optical experiments. These findings should be a general feature of tetrahedral AX_2 amorphous networks.

The high-frequency vibrations in amorphous SiO_2 (a-SiO_2), corresponding to Si–O stretching modes, are responsible for a double peak that is clearly distinguishable in neutron spectra (*1*, *2*). In the same frequency range, infrared (*3*–*5*) and Raman measurements (*6*–*8*) show a LO-TO splitting induced by the long-range nature of the Coulomb fields that are present in ionic materials (*9*, *10*). Because the splittings in neutron and optical spectra are similar, two different explanations for their occurrence have been invoked. The splitting in the neutron spectrum has alternatively been attributed to two different vibrations of molecular subunits (*3*, *11*–*13*), with one of them being optically inactive, or interpreted as a LO-TO effect related to a single type of stretching mode (*14*, *15*).

The explanation in terms of a separation between LO and TO modes arises naturally as an extension from crystalline SiO_2. In α quartz, at the Γ point of the Brillouin zone, a splitting of about 20 meV between LO and TO phonon modes is indisputable (*16*, *17*). De Leeuw and Thorpe showed that the LO-TO splitting as observed in infrared spectra (that is, for a long-wavelength excitation) could be generalized to an amorphous system (*9*). However, their model failed to reproduce the double peak in the vibrational density of states that is observed with neutron scattering

---

J. Sarnthein, Institut Romand de Recherche Numérique en Physique des Matériaux (IRRMA), IN-Ecublens, CH-1015 Lausanne, Switzerland.
A. Pasquarello and R. Car, IRRMA, IN-Ecublens, CH-1015 Lausanne, Switzerland, and Department of Condensed Matter Physics, University of Geneva, CH-1211 Geneva, Switzerland.

*To whom correspondence should be addressed.

(*1*). In α quartz, a similar splitting in the vibrational density of states also appears (*18*), but the one-to-one relation of the integrated areas under the peaks indicates that an explanation based on the LO-TO effect only cannot be sufficient. Furthermore, comparison between the spectra of glass and silica polymorphs does not support a LO-TO interpretation (*11*).

Following a different line of reasoning, Sen and Thorpe described the vibrational properties of the amorphous network departing from the molecular modes of its tetrahedral subunits (*19*). However, because of the rather large Si–O–Si angle connecting the SiO$_4$ subunits in *a*-SiO$_2$, the molecular modes are expected to intermix strongly, making it difficult to predict the actual spectrum in the absence of a realistic model (*19*). Nevertheless, the decomposition into molecular modes has often been pursued (*12, 13, 20*).

Despite the accuracy of current first-principles approaches in reproducing the vibrational properties of crystalline SiO$_2$ (*17, 18*), the understanding of such properties of *a*-SiO$_2$ has remained far less developed. The essential difficulty in the latter case consists in the determination of the amorphous structure, which is an essential prerequisite to the calculation of the vibrational spectrum. The vibrational spectra of *a*-SiO$_2$ obtained with the use of different empirical potentials (*9, 21, 22*) differ significantly from each other and from experimental results, although refined models can be in good agreement with experimental results (*12, 13*). To avoid the dependence on empirical parameters, we use here a first-principle scheme.

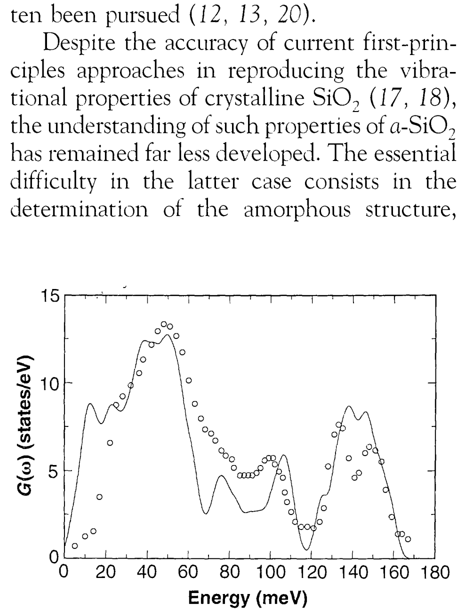

Fig. 1. Calculated effective density of states $G(\omega)$ (solid line) compared to neutron scattering data from (*1*) (circles). The calculated $G(\omega)$ was obtained with the use of the atomic structure factors $b_{Si} = 4.149$ fm and $b_O = 5.803$ fm (*29*) and is convoluted with a Gaussian of width $\sigma = 2.5$ meV.

We studied the vibrational properties of *a*-SiO$_2$ within the local density approximation to density functional theory. We adopted a model structure previously obtained (*23*) with a quench from the melt using first-principles molecular dynamics (*24, 25*). This structure consists of $n = 72$ atoms whose atomic positions were fully relaxed at the experimental density (2.20 g/cm^3), in a periodically repeated cubic cell. Only valence electrons were explicitly considered; pseudopotentials were used to account for core-valence interactions. A plane-wave basis set was used for both the electronic wave functions and charge density (*26*).

The second derivatives of the total energy with respect to atomic displacements were calculated numerically by taking finite differences of the atomic forces. The vibrational frequencies and their corresponding eigenmodes were obtained by diagonalization of the resulting dynamic matrix. From these quantities, the dynamic structure factor $S(\mathbf{q}, \omega)$ as a function of wave vector **q** and frequency ω and the neutron effective density of states $G(\omega)$ could then be derived (*1, 22*). Comparison of the calculated $G(\omega)$ with the one obtained by inelastic neutron scattering (*1*) (Fig. 1) shows that the agreement between theory and experiment is remarkably good: All the features as well as the relative heights of the peaks are matched by our calculation. Notice in particular that the splitting in the Si–O stretching modes is well reproduced.

In order to distinguish between longitudinal and transverse modes, we define $G_{\parallel}(\omega)$ and $G_{\perp}(\omega)$ similarly to $G(\omega)$ but weighted according to the projections of the eigenmodes onto parallel and orthogonal directions, respectively, with respect to **q**. $G_{\parallel}(\omega)$ and $G_{\perp}(\omega)$ resemble $G(\omega)$, both showing a doublet for the Si–O stretching modes (Fig. 2A). This result arises because the distinction between parallel and orthogonal directions vanishes in the limit of large **q** and because of the predominant weight of these **q**'s in the definition of $G_{\parallel}(\omega)$ and $G_{\perp}(\omega)$. Thus, the LO-TO effect is definitely ruled out as a possible explanation for the doublet in the inelastic neutron spectrum.

For every SiO$_4$ tetrahedral subunit, the four Si–O stretching modes can be transformed into symmetry-adapted combinations belonging to the symmetry group T_d, giving rise to a nondegenerate representation A_1 and to a threefold degenerate representation T_2. The A_1 mode corresponds to an in-phase motion of all the oxygen atoms toward the central Si atom. In the T_2 modes, two oxygen atoms move closer to the central Si atom while the other two move away. To keep the center of mass immobile, the Si atom does not move in the A_1 mode but participates to the T_2 modes. Considering the total density of states $Z(\omega)$ and its projection onto the A_1 and T_2 representations (Fig. 2B), the origin of the doublet in the Si–O modes appears to be associated with the different representations of the tetrahedral subunits, in agreement with previous calculations (*12, 13*). The T_2 modes dominate the low-frequency side of the doublet, whereas the contribution of the A_1 modes is peaked on the high-frequency side of the doublet. The stretching modes completely account for all the modes of $Z(\omega)$ with $\omega > 90$ meV; in particular, the peak at 100 meV is mostly T_2 and corresponds to the motion of the Si atom in response to the Si–O stretching.

In order to clarify the relation between the splitting in the effective density of states $G(\omega)$ and the LO-TO splitting appearing in infrared absorption spectra, we now consider the generalized density of states $G(\mathbf{q}, \omega) \sim \omega S(\mathbf{q}, \omega)/q^2$ in the long-wavelength limit (*27*). By consideration of projections of the eigen-

Fig. 2. (**A**) Effective density of states $G(\omega)$ (dotted line) and its components $G_{\perp}(\omega)$ (solid line) and $G_{\parallel}(\omega)$ (dashed line) resulting from a projection on vibrational modes perpendicular and parallel to **q**. (**B**) Total density of states $Z(\omega)$ (solid line) and its projection on symmetry-adapted modes of the SiO$_4$ tetrahedra A_1 (dashed line) and T_2 (dash-dotted line).

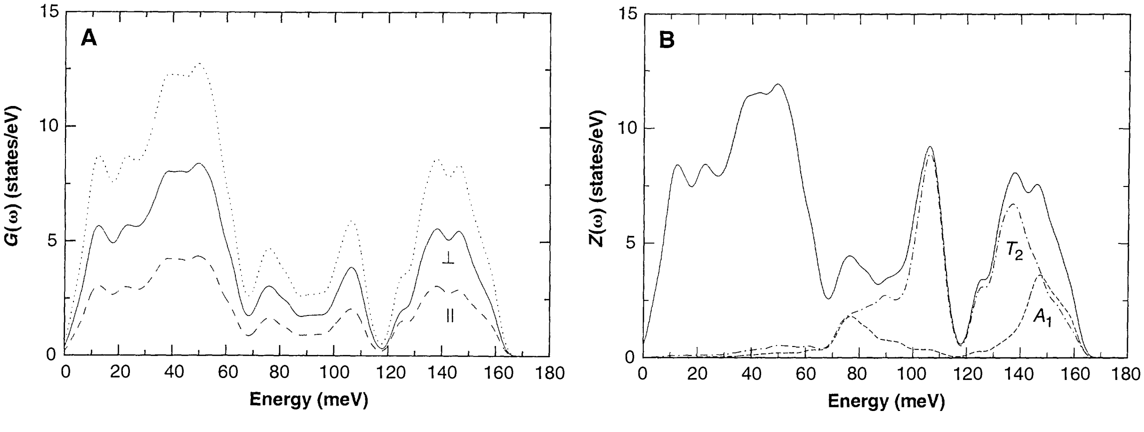

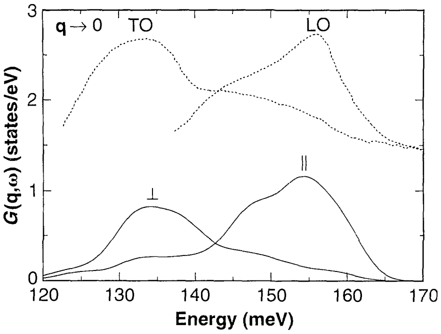

Fig. 3. Generalized density of states $G(\mathbf{q}, \omega)$ in the limit $\mathbf{q} \rightarrow 0$ for longitudinal and transverse excitations (solid lines). The LO and TO infrared absorption spectra (dashed lines) from (*3*) are shown for a qualitative comparison (in arbitrary units and on a semilogarithmic scale to enhance the structure in the shoulders).

modes parallel and orthogonal to the direction of **q**, a longitudinal and a transverse limit, respectively, were obtained (Fig. 3). The appearance of a well-defined splitting related to a LO-TO effect is now apparent. A qualitative comparison with the infrared absorption spectra measured by Kirk (*3*) shows good agreement: The position of the peaks as well as the structure in the wings are very similar in the theoretical and experimental spectra. Note, in particular, that the peak in the calculated longitudinal spectrum appears at higher frequencies than does the upper peak in the total density of states, in agreement with the position of the LO peak in infrared (*3*) and hyper-Raman (*28*) spectra as compared with the position of the upper peak in neutron spectra (*1*). The structure of the peaks can be further analyzed by considering the same long wavelength limit for the A_1 and T_2 projected modes. This reveals that the transverse spectrum originates almost exclusively from T_2 modes, with a vanishingly small contribution from A_1 modes. On the other hand, both modes contribute to the longitudinal spectrum; the A_1 mode contributes only to the principal peak, whereas the T_2 mode contributes both to the principal peak and to the wing at lower frequencies.

This first-principles study of the vibrational properties of a-SiO_2 provides a comprehensive understanding of the origin of the high-frequency doublet appearing in inelastic neutron scattering and its relation with infrared measurements. We expect that such detailed studies will play an important role in the assignment of other unidentified features in the vibrational spectra of amorphous systems.

REFERENCES AND NOTES

1. J. M. Carpenter and D. L. Price, *Phys. Rev. Lett.* **54**, 441 (1985); D. L. Price and J. M. Carpenter, *J. Non-Cryst. Solids* **92**, 153 (1987).
2. A. C. Hannon *et al.*, *J. Non-Cryst. Solids* **150**, 239 (1992); M. Arai *et al.*, *Physica B* **180**, 779 (1992).
3. C. T. Kirk, *Phys. Rev. B* **38**, 1255 (1988).
4. R. M. Almeida, *ibid.* **45**, 161 (1992).
5. C. Martinet and R. A. B. Devine, *J. Appl. Phys.* **77**, 4343 (1995).
6. F. L. Galeener and G. Lucovsky, *Phys. Rev. Lett.* **37**, 1474 (1976).
7. F. L. Galeener, A. J. Leadbetter, M. W. Stringfellow, *Phys. Rev. B* **27**, 1052 (1983).
8. G. E. Walrafen, Y. C. Chu, M. S. Hokmabadi, *J. Chem. Phys.* **92**, 6987 (1990).
9. S. W. de Leeuw and M. F. Thorpe, *Phys. Rev. Lett.* **55**, 2879 (1985); M. F. Thorpe and S. W. de Leeuw, *Phys. Rev. B* **33**, 8490 (1986).
10. M. C. Payne and J. C. Inkson, *J. Non-Cryst. Solids* **68**, 351 (1984).
11. P. McMillan, B. Piriou, A. Navrotsky, *Geochim. Cosmochim. Acta* **46**, 2021 (1982); P. F. McMillan, P. T. Poe, P. Gillet, B. Reynard, *ibid.* **58**, 3653 (1994).
12. R. G. Della Valle and E. Venuti, *Chem. Phys.* **179**, 411 (1994).
13. M. Wilson, P. A. Madden, M. Hemmati, C. A. Angell, *Phys. Rev. Lett.* **77**, 4023 (1996).
14. R. M. Pick and M. Yvinec, in *Lattice Dynamics*, M. Balkanski, Ed. (Flammarion, Paris, 1977), pp. 459–461.
15. A. Lehmann, L. Schumann, K. Hübner, *Phys. Status Solidi B* **117**, 689 (1983).
16. D. Strauch and B. Dorner, *J. Phys. Cond. Matter* **5**, 6149 (1993).
17. X. Gonze, D. C. Allan, M. P. Teter, *Phys. Rev. Lett.* **68**, 3603 (1992); X. Gonze *et al.*, *Phys. Rev. B* **50**, 13035 (1994).
18. C. Lee and X. Gonze, *Phys. Rev. Lett.* **72**, 1686 (1994); *Phys. Rev. B* **51**, 8610 (1995).
19. P. N. Sen and M. F. Thorpe, *Phys. Rev. B* **15**, 4030 (1977).
20. F. L. Galeener, *ibid.* **19**, 4292 (1979).
21. R. J. Bell and D. C. Hibbins-Butler, *J. Phys. C: Solid State Phys.* **8**, 787 (1975).
22. W. Jin, P. Vashishta, R. K. Kalia, J. P. Rino, *Phys. Rev. B* **48**, 9359 (1993).
23. J. Sarnthein, A. Pasquarello, R. Car, *Phys. Rev. Lett.* **74**, 4682 (1995); *Phys. Rev. B* **52**, 12690 (1995).
24. R. Car and M. Parrinello, *Phys. Rev. Lett.* **55**, 2471 (1985).
25. A. Pasquarello, K. Laasonen, R. Car, C. Lee, D. Vanderbilt, *ibid.* **69**, 1982 (1992); K. Laasonen, A. Pasquarello, R. Car, C. Lee, D. Vanderbilt, *Phys. Rev. B* **47**, 10142 (1993).
26. Compared to (*23*), we used improved basis sets with cutoffs of 24 and 200 rydbergs for the electronic wave functions and charge density, respectively.
27. We used the smallest finite **q** allowed by our periodic boundary conditions, avoiding the need for depolarizing fields (*9*).
28. V. N. Denisov *et al.*, *J. Non-Cryst. Solids* **64**, 195 (1984).
29. S. Susman *et al.*, *Phys. Rev. B* **43**, 1194 (1991).
30. The authors thank A. Dal Corso and X. Gonze for useful discussions. Partially supported by the Swiss National Science Foundation. The calculations were performed at the Swiss Scientific Computing Center (CSCS).

21 November 1996; accepted 29 January 1997

Signaling by Phosphoinositide-3,4,5-Trisphosphate Through Proteins Containing Pleckstrin and Sec7 Homology Domains

Jes K. Klarlund, Adilson Guilherme, John J. Holik,
Joseph V. Virbasius, Anil Chawla, Michael P. Czech*

Signal transmission by many cell surface receptors results in the activation of phosphoinositide (PI) 3-kinases that phosphorylate the 3′ position of polyphosphoinositides. From a screen for mouse proteins that bind phosphoinositides, the protein GRP1 was identified. GRP1 binds phosphatidylinositol-3,4,5-trisphosphate [PtdIns(3,4,5)P_3] through a pleckstrin homology (PH) domain and displays a region of high sequence similarity to the yeast Sec7 protein. The PH domain of the closely related protein cytohesin-1, which, through its Sec7 homology domain, regulates integrin β2 and catalyzes guanine nucleotide exchange of the small guanine nucleotide–binding protein ARF1, was also found to specifically bind PtdIns(3,4,5)P_3. GRP1 and cytohesin-1 appear to connect receptor-activated PI 3-kinase signaling pathways with proteins that mediate biological responses such as cell adhesion and membrane trafficking.

Cellular 3-phosphoinositides are generated through the actions of a family of PI 3-kinases and appear to have regulatory roles in multiple cell functions. In yeast the Vps34 gene product, a PI 3-kinase with substrate specificity restricted to phosphatidylinositol (PtdIns), is required for correct sorting of carboxypeptidase Y to the vacuole (*1*). In mammalian cells three classes of PI 3-kinases have been identified in addition to a Vps34 homolog (*2*). These include p110 isoforms regulated by p85 subunits containing SRC homology 2 (SH2) domains (*3*), a p110γ PI 3-kinase regulated by heterotrimeric guanine nucleotide–binding proteins (*4*), and a PI 3-kinase containing a homology domain (C2 domain) thought to bind membrane lipids (*5*). The p85-p110 and p110γ type PI 3-kinases that are specifically activated by receptor signaling systems exhibit broad substrate specificities, and their activation leads to rapid phosphorylation of the inositol D-3 positions on PtdIns, PtdIns-4-phosphate [PtdIns(4)P], and

---

Program in Molecular Medicine and Department of Biochemistry and Molecular Biology, University of Massachusetts Medical Center, 373 Plantation Street, Worcester, MA 01605, USA.

*To whom correspondence should be addressed.